AppliedMath

MDPI

Article

Optimization of Plate Vibration Based on Innovative Elliptical Thickness Variation

Neeraj Lather [1], Naveen Mani [2], Rahul Shukla [3,*] and Amit Sharma [1]

[1] Department of Mathematics, Amity University Haryana, Gurugram 122413, India; latherneeraj69@gmail.com (N.L.); dba.amitsharma@gmail.com (A.S.)
[2] Department of Mathematics, Chandigarh University, Mohali 140301, India; naveenmani81@gmail.com or naveen.e10461@cumail.in
[3] Department of Mathematical Sciences and Computing, Walter Sisulu University, Mthatha 5117, South Africa
* Correspondence: rshukla@wsu.ac.za or rshukla.vnit@gmail.com

Abstract: This study innovatively explores vibrational control with reference to elliptical thickness variation. Traditionally, plate vibrations have been analysed by incorporating circular, linear, parabolic, and exponential thickness variations. However, these variations often fall short in optimizing vibrational characteristics. So, we develop a new formula specifically for orthotropic as well as isotropic plates with elliptical thickness profiles and employ the Rayleigh–Ritz method to calculate the vibrational frequencies of the plate. This research demonstrates that elliptical variation significantly reduces vibrational frequencies compared to conventional thickness profiles. The findings indicate that this unique configuration enhances vibrational control, offering potential applications in engineering fields where vibration reduction is essential. The results provide a foundation for further exploration of non-standard thickness variations in the design of advanced structural components. The study reveals that the elliptical variation in tapering parameter is a much better choice than other variation parameters studied in the literature for the purpose of optimizing the vibrational frequency of plates.

Keywords: optimization; vibration; rectangle plate; thickness

MSC: 74K20; 74H50

check for updates

Academic Editor: Takayuki Hibi

Received: 7 March 2025
Revised: 14 April 2025
Accepted: 21 May 2025
Published: 29 May 2025

Citation: Lather, N.; Mani, N.; Shukla, R.; Sharma, A. Optimization of Plate Vibration Based on Innovative Elliptical Thickness Variation. *AppliedMath* **2025**, *5*, 63. https://doi.org/10.3390/appliedmath5020063

Copyright: © 2025 by the authors. Licensee MDPI, Basel, Switzerland. This article is an open access article distributed under the terms and conditions of the Creative Commons Attribution (CC BY) license (https://creativecommons.org/licenses/by/4.0/).

1. Introduction

Plate vibration theory is a branch of structural dynamics that studies how plates respond to external forces and undergo vibratory motion. The vibrations can be caused by various factors, plate thickness, thermal effects, or fluid interactions. The analysis of plate vibration is crucial in engineering fields, such as mechanical, civil, and aerospace engineering, where the behaviour of structural elements under dynamic loading needs to be understood for design and safety purposes. Vibration control in plate structures is a critical concern in various engineering applications, where excessive vibrations can lead to structural failure or performance issues. Traditionally, thickness variations such as circular, linear, and parabolic profiles have been used to address these challenges, yet they often fail to optimize vibrational characteristics effectively. This study introduces a novel elliptical thickness variation that significantly enhances the control of plate vibrations. We observe that plates with elliptical thickness exhibit lower vibrational frequencies compared to those with conventional profiles. This innovative variation in thickness not only improves vibrational performance but also opens new avenues for research and application in fields

requiring advanced structural design. By exploring the benefits of elliptical thickness variations, this work aims to contribute to the development of more efficient and robust engineering solutions.

The weak-form quadrature element method [1] for free vibration analysis of thin sectorial plates, addressing vertex stress singularities through analytical displacement descriptions, has been discussed and a generalized eigenvalue formulation thereof has been established, providing frequencies for different plate parameters. A double Legendre polynomial quadrature-free method [2] was analyzed for axisymmetric free vibrations in FG piezoelectric circular plates, incorporating boundary conditions directly. The method was validated against the literature and COMSOL, showing how the material gradient index and radius–thickness ratio affect resonant frequencies. Vibration analysis of functionally graded circular plates with variable thickness in a thermal environment was conducted using the Generalized Differential Quadrature Method [3]. The effects of taper constant, volume fraction index, and temperature difference on natural frequencies were examined and validated against the existing literature. A study of vibration of rectangular thin plates (free edges) with elastic foundations using the symplectic superposition method [4] was proposed and it was shown that this approach involved transforming the problem into two sub-problems, with solutions validated against specific plate frequencies and mode functions. An improved refined shear and normal deformation theory is analyzed in [5] for the vibration behavior of FG rectangular plates using a three-unknown displacement field. The results closely match more complex solutions, enabling a comprehensive study of static and dynamic behavior while reducing the number of variables. The electro-thermomechanical vibrational behavior of FG piezoelectric plates with porosities using a refined four-variable plate theory is examined in [6] and the effects of temperature changes, applied voltage, and boundary conditions are discussed, offering insights for designing smart structures. The free vibration and stress of an annular plate made of saturated porous materials using first-order shear deformation theory [7] were studied and it was demonstrated that increased porosity reduced stiffness, frequency, and stresses, providing insights for designing structures with targeted mechanical properties. An adaptive finite element method [8] was implemented for free vibration analysis of plates with arbitrary thickness variations using Carrera's unified formulation, allowing for kinematic adaptation to complex geometries, and it was shown that these elements enabled accurate analysis of innovative structures with significantly fewer degrees of freedom compared to classical 3D finite elements. A high-accuracy solution is introduced in [9] for the in-plane vibrations of rectangular plates, covering all edge restraint combinations using series to solve coupled differential equations. Benchmark results for square orthotropic plates were compared with known and approximate solutions. Exact solutions for free vibrations of clamped rectangular plates using asymptotic analysis of infinite systems were studied in [10]; the quasi-regularity of the system was proved and an algorithm was presented for determining natural frequencies, supported by numerical examples. A mathematical model is introduced in [11,12] to explore the influence of temperature on the vibrational frequency of an isotropic rectangular plate using the Rayleigh–Ritz method; the authors computed the first two natural frequencies across diverse boundary conditions for various plate parameter values.

The free vibration behavior of porous FG nanoplates supported by an elastic foundation using the Rayleigh–Ritz approach is analysed in [13]. The aim of the study was to design and optimize advanced nanomaterials for engineering applications. Free in-plane vibrations of rectangular sheets under various boundary conditions using an enhanced Rayleigh–Ritz method were explored in [14] to investigate how changes in geometric parameters affect the free vibrations of rectangular sheets. In [15], the free vibration and

buckling behaviors of an FG nanoplate supported by a Winkler–Pasternak foundation are investigated to examine the effects of edge constraints, aspect ratios, material properties, nonlocal parameters, and foundation parameters on the frequency and buckling load. A numerical thermoelastic vibrational analysis (first two modes) of bi-exponential tapered triangular plates (isosceles right-angle, right-angle, acute, and obtuse) under exponential thermal conditions and varying structural parameters on fully clamped and fully simply supported edges is conducted in [16] using the Rayleigh–Ritz method.

In the present investigation, the dynamic behaviour of a nonuniform rectangular plate subjected to a thermal field is analyzed. The plate is modeled with elliptic variation in thickness and parabolic variation in temperature distribution along both coordinate directions. The Rayleigh–Ritz method is applied to derive the governing frequency equation, and the fundamental first and second mode of vibration are computed for different values of thickness variation, thermal gradient, and aspect ratio.

2. Analysis

In this section, we will describe the geometry of the plate and the governing differential equation of the model, as well as limitations/assumptions made in the model.

2.1. Geometry of the Plate

In the present study, the behaviour of a rectangular plate with elliptically varying thickness l (as shown in Figure 1) along one direction that is also subjected to bi-parabolic temperature variation τ along both directions is studied. The plate is considered to have a constant Poisson's ratio ν and uniform density ρ. The domain of the plate in the $\zeta\psi$-plane is defined by $0 \leqslant \zeta \leqslant a$ and $0 \leqslant \psi \leqslant b$, where a and b denote the plate's length and breadth, respectively.

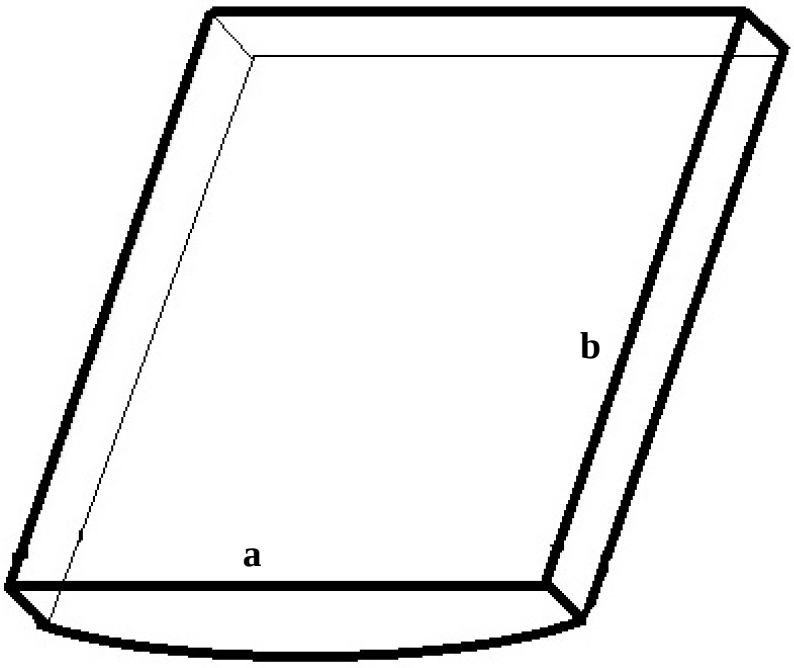


Figure 1. Rectangle plate with elliptical variation in tapering in one dimension.

2.2. Governing Differential Equation of Motion of Isotropic Rectangle Plate

The differential equation of motion for the isotropic plate is taken from [17]:

$$\frac{\partial^2 M_\zeta}{\partial \zeta^2} + 2\,\frac{\partial^2 M_{\zeta\psi}}{\partial \zeta \partial \psi} + \frac{\partial^2 M_\psi}{\partial \psi^2} = \rho\, l\, \frac{\partial^2 \phi}{\partial t^2}. \tag{1}$$

where M_ζ and M_ψ give the bending moment per unit length in the ζ and ψ directions, which resist bending along their respective directions. $M_{\zeta\psi}$ is the twisting moment in the $\zeta\psi$ direction, which resists twisting caused by combined bending. ρ is the material density, l is the plate thickness, ϕ is the deflection, and t is time. The expressions of M_ζ, M_ψ, and $M_{\zeta\psi}$ are given as follows as discussed in [17]:

$$M_\zeta = -D_1\left[\frac{\partial^2\phi}{\partial\zeta^2} + \nu\frac{\partial^2\phi}{\partial\psi^2}\right]. \tag{2}$$

$$M_\psi = -D_1\left[\nu\frac{\partial^2\phi}{\partial\zeta^2} + \frac{\partial^2\phi}{\partial\psi^2}\right], \tag{3}$$

$$M_{\zeta\psi} = -D_1(1-\nu)\left[\frac{\partial^2\phi}{\partial\zeta\partial\psi}\right]. \tag{4}$$

where $D_1 = \left(\frac{El^3}{12\,(1-\nu^2)}\right)$ is the flexural rigidity (i.e., the plate's resistance to bending), which indicates how stiff the plate is when bending load is applied. Here, E and ν represent the Young's modulus and Poisson's ratio of the plate, respectively.

Using Equations (2)–(4) in Equation (1), we obtain

$$\begin{aligned}\Bigg[D_1\left(\frac{\partial^4\phi}{\partial\zeta^4} + 2\frac{\partial^4\phi}{\partial\zeta^2\partial\psi^2} + \frac{\partial^4\phi}{\partial\psi^4}\right) + 2\frac{\partial D_1}{\partial\zeta}\left(\frac{\partial^3\phi}{\partial\zeta^3} + \frac{\partial^3\phi}{\partial\zeta\partial\psi^2}\right) + 2\frac{\partial D_1}{\partial\psi}\left(\frac{\partial^3\phi}{\partial\zeta^2\partial\psi} + \frac{\partial^3\phi}{\partial\psi^3}\right)\\ + \frac{\partial^2 D_1}{\partial\zeta^2}\left(\frac{\partial^2\phi}{\partial\zeta^2} + \nu\frac{\partial^2\phi}{\partial\psi^2}\right) + \frac{\partial^2 D_1}{\partial\psi^2}\left(\frac{\partial^2\phi}{\partial\psi^2} + \nu\frac{\partial^2\phi}{\partial\zeta^2}\right) + 2\left(1-\nu\right)\frac{\partial^2 D_1}{\partial\zeta\partial\psi}\frac{\partial^2\phi}{\partial\zeta\partial\psi}\Bigg] + \rho\, l\,\frac{\partial^2\phi}{\partial t^2} = 0.\end{aligned} \tag{5}$$

For the solution of Equation (5), we write $\phi(\zeta,\psi,t)$ as

$$\phi(\zeta,\psi,t) = \Phi(\zeta,\psi)\times T(t), \tag{6}$$

where $\Phi(\zeta,\psi)$ is known as the deflection function of the plate, which determines how much the plate will deform under certain load conditions, and $T(t)$ is the time function.

Substituting Equation (6) in (5), we obtain

$$\begin{aligned}\Bigg[D_1\left(\frac{\partial^4\Phi}{\partial\zeta^4} + 2\frac{\partial^4\Phi}{\partial\zeta^2\partial\psi^2} + \frac{\partial^4\Phi}{\partial\psi^4}\right) + 2\frac{\partial D_1}{\partial\zeta}\left(\frac{\partial^3\Phi}{\partial\zeta^3} + \frac{\partial^3\Phi}{\partial\zeta\partial\psi^2}\right) + 2\frac{\partial D_1}{\partial\psi}\left(\frac{\partial^3\Phi}{\partial\zeta^2\partial\psi} + \frac{\partial^3\Phi}{\partial\psi^3}\right)\\ + \frac{\partial^2 D_1}{\partial\zeta^2}\left(\frac{\partial^2\Phi}{\partial\zeta^2} + \nu\frac{\partial^2\Phi}{\partial\psi^2}\right) + \frac{\partial^2 D_1}{\partial\psi^2}\left(\frac{\partial^2\Phi}{\partial\psi^2} + \nu\frac{\partial^2\Phi}{\partial\zeta^2}\right) + 2\left(1-\nu\right)\frac{\partial^2 D_1}{\partial\zeta\partial\psi}\frac{\partial^2\Phi}{\partial\zeta\partial\psi}\Bigg]/\rho\, l\,\Phi = -\frac{1}{T}\frac{\partial^2 T}{\partial t^2}.\end{aligned} \tag{7}$$

Both sides of the Equation (7) are independent of each other. As a result, it holds true if both sides are equal to the same positive constant—say, ω^2. In that case from LHS of Equation (7), we obtain

$$\begin{aligned}\Bigg[D_1\left(\frac{\partial^4\Phi}{\partial\zeta^4} + 2\frac{\partial^4\Phi}{\partial\zeta^2\partial\psi^2} + \frac{\partial^4\Phi}{\partial\psi^4}\right) + 2\frac{\partial D_1}{\partial\zeta}\left(\frac{\partial^3\Phi}{\partial\zeta^3} + \frac{\partial^3\Phi}{\partial\zeta\partial\psi^2}\right) + 2\frac{\partial D_1}{\partial\psi}\left(\frac{\partial^3\Phi}{\partial\zeta^2\partial\psi} + \frac{\partial^3\Phi}{\partial\psi^3}\right)\\ + \frac{\partial^2 D_1}{\partial\zeta^2}\left(\frac{\partial^2\Phi}{\partial\zeta^2} + \nu\frac{\partial^2\Phi}{\partial\psi^2}\right) + \frac{\partial^2 D_1}{\partial\psi^2}\left(\frac{\partial^2\Phi}{\partial\psi^2} + \nu\frac{\partial^2\Phi}{\partial\zeta^2}\right) + 2\left(1-\nu\right)\frac{\partial^2 D_1}{\partial\zeta\partial\psi}\frac{\partial^2\Phi}{\partial\zeta\partial\psi}\Bigg] = \rho\, l\,\Phi\omega^2\end{aligned} \tag{8}$$

where Equation (8) represents the equation of motion for the isotropic rectangle plate.

2.3. Assumptions Made in the Problem

Analyzing the vibrations of structures is a complex task due to the variation in structural properties. To ensure a more precise and manageable prediction of vibration behavior, we make certain assumptions. These predefined limitations form the basis of the current model and support its detailed examination.

To strike a balance between structural integrity and cost-effectiveness, engineering applications often utilize plates of varying thickness. These plates play a crucial role in the design of turbine blades, bridge panels, and airplane fans, optimizing both performance and efficiency. In order to investigate the effect of nonlinear thickness variation on the vibrational behaviour of plates, we developed a new formula for one-dimensional elliptical thickness. The new devloped formula is formulated as

$$l = l_0\left\{1+\beta\left(\frac{b}{a}-\frac{b}{a}\sqrt{1-\frac{\zeta^2}{a^2}}\right)\right\} \tag{9}$$

where l_0 is the thickness at the origin and $\beta(0 \leqslant \beta \leqslant 1)$ is the tapering parameter (refer to Figure 1).

Structures often function in environments with elevated temperatures, where temperature distribution varies across different points within the system. These fluctuations significantly influence the vibrational characteristics of the structure. As a result, understanding and analyzing the impact of temperature on structural vibrations becomes crucial for ensuring stability and performance. In this study, we assume that the plate experiences a temperature distribution. For this, a two-dimensional parabolic temperature distribution is taken into account as in [17]:

$$\tau = \tau_0\left(1-\zeta^2/a^2\right)\left(1-\psi^2/b^2\right), \tag{10}$$

where τ and τ_0 denote the temperature on and at the origin, respectively.

For isotropic materials, the modulus of elasticity is given as discussed in [18]

$$E = E_0(1-\gamma\tau) \tag{11}$$

where E_0 is the Young's modulus and γ is called the slope of variation.

Using Equation (10) and implementing the non-dimensional variable $\zeta_1 = \zeta/a, \psi_1 = \psi/a$, Equation (11) becomes

$$E = E_0\left(1-\alpha\left(1-\zeta_1^2\right)\left(1-\frac{a^2\psi_1^2}{b^2}\right)\right) \tag{12}$$

where $\alpha = \gamma\tau_0 (0 \leq \alpha < 1)$ is called the thermal gradient.

3. Solution for Frequency

In order to find the frequency equation, we use the Rayleigh–Ritz technique, as given in [19]:

$$L = \delta(V_s - T_s) = 0. \tag{13}$$

where V_s and T_s give the strain energy and kinetic energy, expressed as

$$T_s = \frac{1}{2}\rho\omega^2\int_0^1\int_0^{b/a} l\Phi^2 d\psi_1 d\zeta_1 \tag{14}$$

$$V_s = \frac{1}{2}\int_0^1 \int_0^{b/a} D_1 \left[\left(\frac{\partial^2\Phi}{\partial\zeta_1}\right)^2 + \left(\frac{\partial^2\Phi}{\partial\psi_1}\right)^2 + 2\nu\frac{\partial^2\Phi}{\partial\zeta_1^2}\frac{\partial^2\Phi}{\partial\psi_1^2} + 2(1-\nu)\left(\frac{\partial^2\Phi}{\partial\zeta_1\partial\psi_1}\right)^2 \right] d\psi d\zeta \tag{15}$$

where Φ is the deflection function, ω gives the natural frequency, and D_1 is the flexural rigidity, which is given by

$$D_1 = E_0 {l_0}^3 \left(1 - \alpha\left(1-\zeta_1^2\right)\left(1 - \frac{a^2\psi_1^2}{b^2}\right)\right)\left\{1 + \beta\left(\frac{b}{a} - \frac{b}{a}\sqrt{1-\zeta_1}\right)\right\}^3 / 12\left(1-\nu^2\right)$$

Using Equations (13)–(15), we obtain the functional equation

$$L = \frac{1}{2}\int_0^1 \int_0^{b/a} D_1 \left[\left(\frac{\partial^2\Phi}{\partial\zeta_1}\right)^2 + \left(\frac{\partial^2\Phi}{\partial\psi_1}\right)^2 + 2\nu\frac{\partial^2\Phi}{\partial\zeta_1^2}\frac{\partial^2\Phi}{\partial\psi_1^2} + 2(1-\nu)\left(\frac{\partial^2\Phi}{\partial\zeta_1\partial\psi_1}\right)^2 \right] d\psi_1 d\zeta_1 \tag{16}$$
$$- \frac{1}{2}\omega^2\rho\int_0^a \int_0^b l\Phi^2 d\psi_1 d\zeta_1 = 0.$$

After substituting the value of D_1, the functional in Equation (16) becomes

$$L = \frac{D_0}{2}\int_0^1 \int_0^{\frac{b}{a}} \left[\left(1 - \alpha\left(1-\zeta_1^2\right)\left(1 - \frac{a{\psi_1}^2}{b}\right)\right)\left\{1 + \beta\left(\frac{b}{a} - \frac{b}{a}\sqrt{1-\zeta_1}\right)\right\}^3 \right. \tag{17}$$
$$\left. \times \left\{ \left(\frac{\partial^2\Phi}{\partial{\zeta_1}^2}\right)^2 + \left(\frac{\partial^2\Phi}{\partial{\psi_1}^2}\right)^2 + 2\nu\frac{\partial^2\Phi}{\partial{\zeta_1}^2}\frac{\partial^2\Phi}{\partial{\psi_1}^2} + 2(1-\nu)\left(\frac{\partial^2\Phi}{\partial\zeta_1\partial\psi_1}\right)^2 \right\} \right] d\psi_1 d\zeta_1$$
$$- \lambda^2 \int_0^1 \int_0^{\frac{b}{a}} \left[\left\{ 1 + \beta\left(\frac{b}{a} - \frac{b}{a}\sqrt{1-\zeta_1}\right)\right\} \right] \Phi^2 d\psi_1 d\zeta_1 = 0,$$

where

$$D_0 = \left(\frac{E_0 l_0^3}{12\left(1-\nu^2\right)}\right) \text{ and } \lambda^2 = \frac{12a^4\rho\omega^2\left(1-\nu^2\right)}{E_0 {l_0}^2}$$

In this study, we consider the case where the plates are clamped along the four edges; so, the boundary conditions for the clamped edges are taken as in [19]: $\Phi = \Phi_{\zeta_1} = 0,\ \zeta_1 = 0,$ $a, \Phi = \Phi_{\psi_1} = 0, \psi_1 = 0, b$

In order to satisfy the above condition, we choose the following deflection function:

$$\Phi(\zeta_1, \psi_1) = \left[(\zeta_1)^2 (\psi_1)^2 (1-\zeta_1)^2 \left(1 - \frac{a\psi_1}{b}\right)^2 \right] \tag{18}$$
$$\times \left[\sum_{i=0}^{1} \Psi_i \left\{ (\zeta_1)(\psi_1)(1-\zeta_1)\left(1 - \frac{a\psi_1}{b}\right)\right\}^i \right]$$

where $\Psi_i, i = 0, 1$ are arbitrary unknowns.

Now, substituting Equation (18) in Equation (17), and to minimize the functional in Equation (17), we impose the following condition:

$$\frac{\partial L}{\partial \Psi_i} = 0, \quad i = 0, 1. \tag{19}$$

After simplifying (19) for $i = 0, 1$, we obtain

$$Q_{11}\Psi_1 + Q_{12}\Psi_2 = 0; \quad Q_{21}\Psi_1 + Q_{22}\Psi_2 = 0; \tag{20}$$

A non-trivial solution requires the determinant of the coefficient matrix in (20) to be zero. As a result, the frequency equation is formulated as follows:

$$\begin{vmatrix} Q_{11} & Q_{22} \\ Q_{21} & Q_{22} \end{vmatrix} = 0 \tag{21}$$

After solving Equation (21), we obtain the frequency modes of the plate.

4. Numerical Results and Discussion

In this section, we present the numerical and graphical results obtained from the analysis of plate vibrations based on the Rayleigh–Ritz method and calculate the vibrational frequencies (first two modes) for different variations of plate parameters (i.e., thickness variation: elliptical; temperature variation: parabolic; aspect ratio: a/b). In this study, we consider three different cases that will be discussed one by one in the coming paragraphs. The values of the parameters used in calculation are as follows: $E_0 = 7.08 \times 10^{10} \frac{N}{m^2}, v = 0.345,\ l_0 = 0.01$ m, $\rho = 2.80 \times 10^3 \frac{kg}{m^3}$. Detailed analyses of the above cases are as follows:

Case I: In the first scenario, we changed the β from 0.0 to 1.0 for fixed α values (i.e., $\alpha = 0.0, 0.4, 0.8$) and observed that frequency increased as β increased from 0.0 to 1.0, as shown in Table 1. We provide the graphical representation of Table 1 (see Figure 2) for the above-mentioned scenario and note that there was an increase in frequency modes of the plate, through rate of increase was quite small.

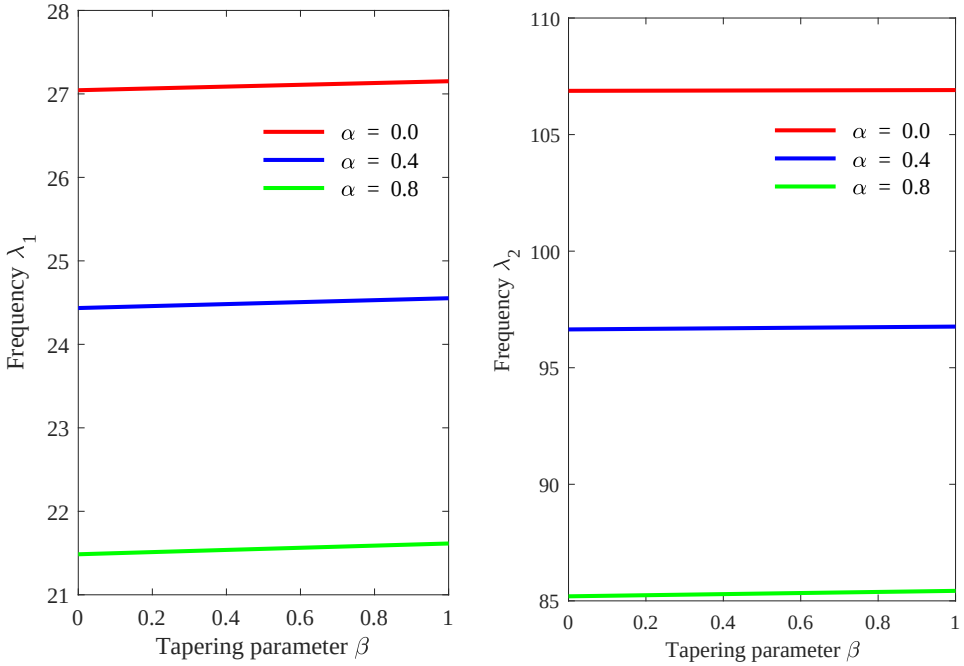


Figure 2. Frequency of rectangle plate vs. tapering parameter β.

Case II: In the second scenario, we varied α from 0.0 to 0.8, for a fixed values of β (i.e., $\beta = 0.0, 0.4, 0.8$, and observed that frequency decreased as the thermal gradient α increased from 0.0 to 0.8, as shown in Table 2 and Figure 3. We also provide a zoomed-in figure of Table 2 (see Figure 4) for the above-mentioned scenario for better visualization of the results, and we note that the rate of change in frequency modes is high corresponding to the thermal gradient α in comparison to frequency modes obtained corresponding to the tapering parameter β.

Table 1. Frequency of rectangle plate vs. tapering parameter β.

	$\alpha = 0.0$		$\alpha = 0.4$		$\alpha = 0.8$	
β	λ_1	λ_2	λ_1	λ_2	λ_1	λ_2
0.0	27.04405	106.8763	24.43494	96.64258	21.48535	85.19486
0.2	27.06581	106.8830	24.45867	96.66707	21.51144	85.24220
0.4	27.08747	106.8896	24.48228	96.69146	21.53739	85.28930
0.6	27.10903	106.8963	24.50577	96.71575	21.56320	85.33614
0.8	27.13049	106.9029	24.52916	96.73995	21.58887	85.38275
1.0	27.15186	106.9096	24.55243	96.76403	21.61440	85.42912

Table 2. Frequency of rectangle plate vs. thermal gradient α.

	$\beta = 0.0$		$\beta = 0.4$		$\beta = 0.8$	
α	λ_1	λ_2	λ_1	λ_2	λ_1	λ_2
0.0	27.04405	106.8763	27.08747	106.8896	27.13049	106.9029
0.2	25.77446	101.8875	25.81975	101.9177	25.86461	101.9476
0.4	24.43494	96.64258	24.48228	96.69146	24.52916	96.73995
0.6	23.01169	91.09765	23.06127	91.16770	23.11034	91.23709
0.8	21.48535	85.19486	21.53739	85.28930	21.58887	85.38275

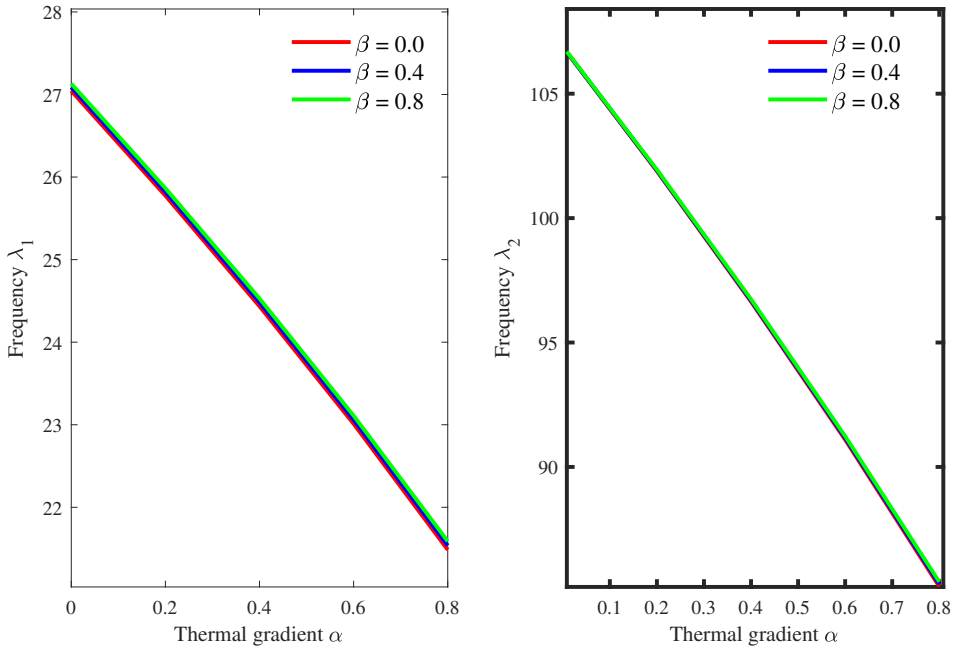


Figure 3. Frequency of rectangle plate vs. thermal gradient α.

Case III: In the last scenario, we varied $\frac{a}{b}$ from 0.25 to 1.50 for fixed values of β and α (i.e., $\beta = \alpha = 0.0, 0.4, 0.8$) as shown in Table 3 and Figure 5 and noticed that frequency decreased as the aspect ratio $\frac{a}{b}$ increased from 0.25 to 1.50; here, the rate of change in frequency modes is very fast and high in comparison to the frequency obtained corresponding to the thermal gradient α and tapering parameter β.

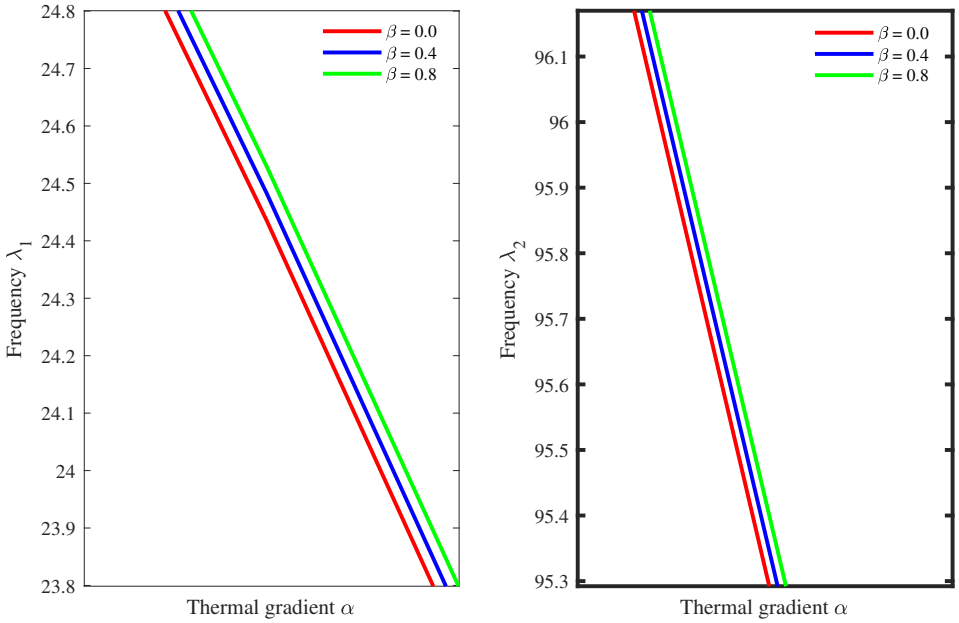


Figure 4. Zoomed-in figure of frequency of rectangle plate vs. thermal gradient α.

Table 3. Frequency of rectangle plate vs. aspect ratio $\frac{a}{b}$.

	$\beta = \alpha = 0.0$		$\beta = \alpha = 0.4$		$\beta = \alpha = 0.8$	
$\frac{a}{b}$	λ_1	λ_2	λ_1	λ_2	λ_1	λ_2
0.25	365.3686	1488.038	348.3270	1425.384	325.1387	1359.022
0.50	98.52109	394.0161	91.38154	365.9131	83.01672	335.7481
0.75	51.07602	200.9572	46.81366	184.0707	41.94837	165.6482
1.0	35.99981	140.8842	32.76909	128.0797	29.11053	113.9718
1.25	29.91236	117.4524	27.12788	106.4049	23.98144	94.16941
1.50	27.04405	106.8763	24.48228	96.69146	21.58887	85.38275

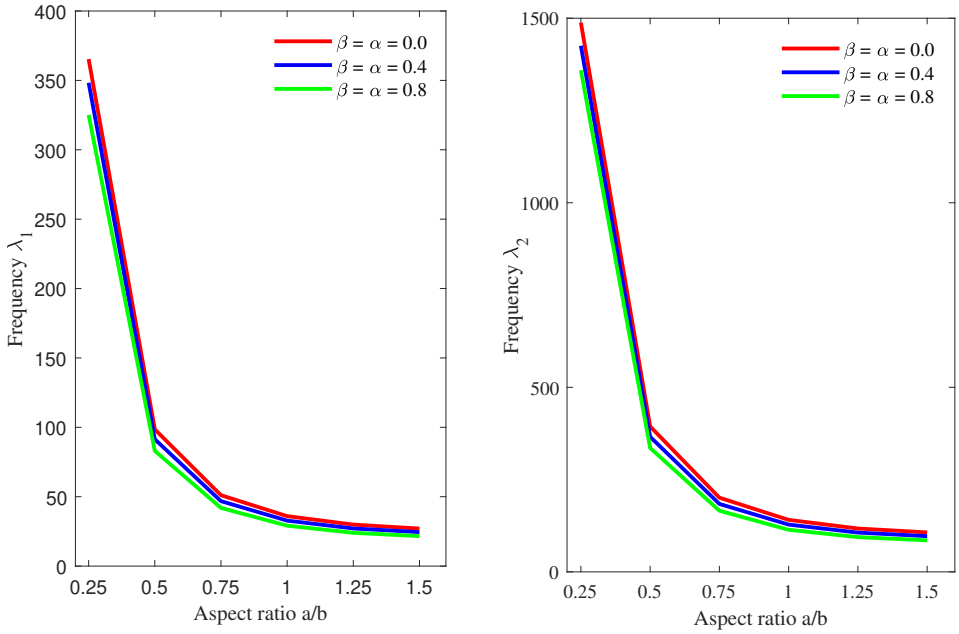


Figure 5. Frequency of rectangle plate vs. aspect ratio a/b.

From the discussion above, we can conclude that the variation (rate of change) in the frequency mode is smaller due to the elliptical variation in the plate parameter. This is because the vibrational frequency takes more time to travel from one end to the other in the case of elliptical variation, compared to the parabolic variation.

5. Comparisons of Frequency Modes

In this section, we perform a comparison of the frequency modes and of the percentage differences between frequency modes that were obtained in the present study with those obtained in [20–23] (see Figure 6 and Table 4, respectively) corresponding to the tapering parameter β.

Figure 6 shows that the frequency obtained in the present study (elliptical tapering) is much smaller compared to the frequencies obtained in [20] (circular tapering), ref. [21] (linear tapering), ref. [22] (exponential tapering), and [23] (parabolic tapering). The frequency mode varies with an increment rate of 0.04% in the present study, which is much smaller compared to the variation in frequency modes achieved in [20] (20.52%), ref. [21] (54.17%), ref. [22] (79.99%), and [23] (35.6%) for the chosen range of the tapering parameter. The physical justification for the reduced vibration is due to the fact that there is more curvature in the elliptical shape as compared to shapes taken earlier (circular tapering, linear tapering, exponential tapering, parabolic tapering, etc.). The fact that the travelling time of the vibrational frequency from one end of the plate to the other takes more time (i.e, the time period of vibration is higher) results in the decay of the variation in frequency modes in comparison to the other considered plate shapes.

Furthermore, Table 4 shows the percentage differences in frequency obtained in the present study and in [20–23]. Table 4 clearly shows that the percentage difference in frequency modes is higher if we choose a circular, linear, exponential, and parabolic variation in the tapering parameter in comparison to the elliptical variation in tapering.

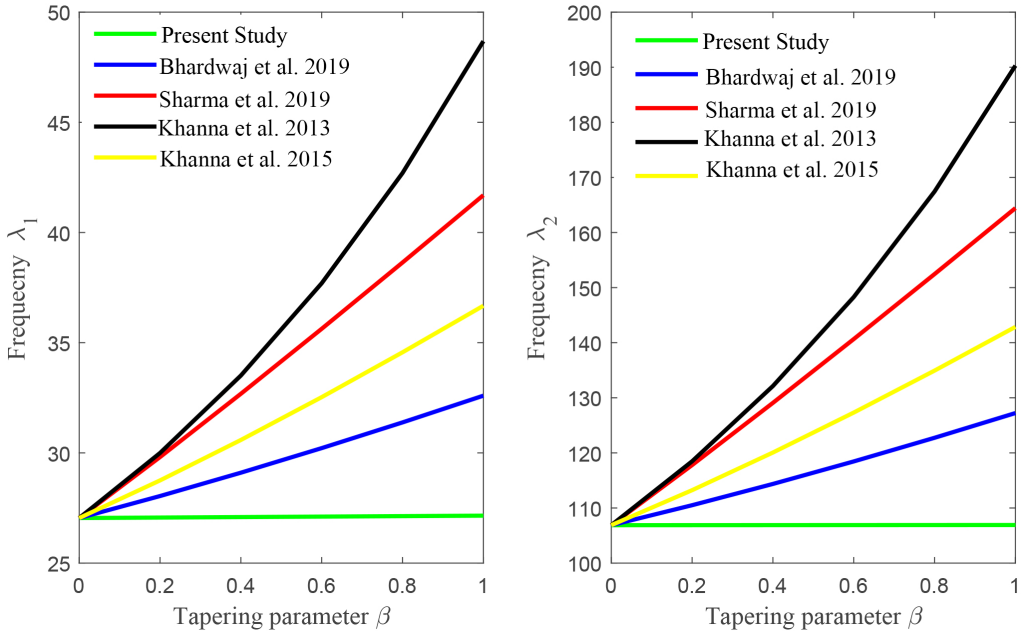


Figure 6. Comparison of frequency modes from the present study with those obtained in [20–23].

Table 4. Percentage difference in frequency modes of the present study with [20–23].

S. No.	Value of Tapering Parameter β	Percentage Difference in Frequency Modes of Present Study with Reference Numbers [20–23]	
1	$\beta = 0.0$	[20]	0%
		[21]	0%
		[22]	0%
		[23]	0%
2	$\beta = 0.6$	[20]	10.85%
		[21]	27.19%
		[22]	32.53%
		[23]	18.18%
3	$\beta = 1.0$	[20]	18.21%
		[21]	42.24%
		[22]	56.76%
		[23]	29.83%

6. Conclusions

The primary aim of this study was to optimize and control vibrational frequency modes in tapered structural systems. Based on the analytical and numerical results, it was concluded that elliptical tapering offers superior performance in minimizing vibrational frequencies compared to circular, linear, exponential, and parabolic tapering profiles. Specifically, elliptical tapering not only reduces the frequency values more effectively but also results in significantly lower fluctuations across different modes, indicating greater dynamic stability. These findings highlight the practical advantage of elliptical tapering in structural design, particularly in applications where vibration control is critical—such as in aerospace structures, precision instruments, high-rise buildings, and mechanical components subject to dynamic loading. The enhanced stability and precision in frequency control make this tapering profile a promising design strategy for vibration-sensitive systems. In future, the authors aim to study and explore the effects of elliptical tapering in composite or functionally graded materials. Also, the authors would like to extend this research to 3D structures or shell geometries with non-uniform tapering.

Author Contributions: All authors; conceptualization, N.M. and N.L.; methodology, N.M.; validation, R.S., N.L. and A.S.; formal analysis, N.M.; investigation, N.L.; resources, R.S.; writin–original draft preparation, N.L.; writing–review and editing, R.S.; visualization, A.S.; supervision, N.M.; project administration, R.S. All authors have read and agreed to the published version of the manuscript.

Funding: This work was supported by the Directorate of Research and Innovation, Walter Sisulu University.

Data Availability Statement: Data are contained within the article.

Conflicts of Interest: The authors declare no conflict of interest.

References

1. Liu, H.; Zhong, H. Transverse free vibration analysis of thin sectorial plates by the weak form quadrature element method. *J. Vib. Control* **2024**, *30*, 5560–5577. [CrossRef]
2. Zhou, H.; Han, K.; Elmaimouni, L.; Wang, X.; Yu, J. Double Legendre polynomial quadrature-free method for axisymmetric vibration of functionally graded piezoelectric circular plates. *J. Vib. Control* **2024**, *30*, 598–615. [CrossRef]

3. Lal, R.; Saini, R. Vibration analysis of functionally graded circular plates of variable thickness under thermal environment by generalized differential quadrature method. *J. Vib. Control* **2020**, *26*, 73–87. [CrossRef]
4. Su, X.; Bai, E. Analytical free vibration solutions of fully free orthotropic rectangular thin plates on two-parameter elastic foundations by the symplectic superposition method. *J. Vib. Control* **2022**, *28*, 3–16. [CrossRef]
5. Monajati, L.; Farid, N.; Farid, M.; Parandvar, H. Free vibration analyses of functionally graded plates based on improved refined shear and normal deformation theory considering thickness stretching effect using Airy stress function. *J. Vib. Control* **2023**, *29*, 2332–2347. [CrossRef]
6. Barati, M.R.; Zenkour, A.M. Electro-thermoelastic vibration of plates made of porous functionally graded piezoelectric materials under various boundary conditions. *J. Vib. Control* **2018**, *24*, 1910–1926. [CrossRef]
7. Bemani Khouzestani, L.; Khorshidvand, A.R. Axisymmetric free vibration and stress analyses of saturated porous annular plates using generalized differential quadrature method. *J. Vib. Control* **2019**, *25*, 2799–2818. [CrossRef]
8. Moruzzi, M.C.; Cinefra, M.; Bagassi, S. Free vibration of variable-thickness plates via adaptive finite elements. *J. Sound Vib.* **2024**, *577*, 118336.
9. Deutsch, A.; Eisenberger, M. Benchmark analytic in-plane vibration frequencies of orthotropic rectangular plates. *J. Sound Vib.* **2022**, *541*, 117248. [CrossRef]
10. Papkov, S.O.; Banerjee, J.R. Free vibration of thick rectangular orthotropic plates with clamped edges- using asymptotic analysis of infinite systems. *J. Sound Vib.* **2021**, *508*, 116209. [CrossRef]
11. Khanna, A.; Singhal, A. Effect of plate's parameters on vibration of isotropic tapered rectangular plate with different boundary conditions. *J. Low Freq. Noise, Vib. Act. Control* **2016**, *35*, 139–151. [CrossRef]
12. Khanna, A.; Singhal, A. Influence of temperature variation on vibration of rectangular plate of visco-elastic material. *World Sci. News* **2020**, *139*, 61–75.
13. Kumar, A.S.; Kumar, S.; Choudhary, P.K.; Gupta, A.; Narayan, A. Free vibration characteristics of elastic foundation-supported porous functionally graded nanoplates using Rayleigh-Ritz approach. *Int. J. Struct. Integr.* **2024**, *15*, 298–321. [CrossRef]
14. Bagheri, A.; Mortezaei, A.; Sayarinejad, M.A. Analysis of free in-plane vibrations of a rectangular plate with various boundary conditions canonical form using the modified Riley-Ritz method. *Results Eng.* **2024**, *21*, 101768. [CrossRef]
15. Singh, P.P.; Azam, M.S. Free vibration and buckling analysis of elastically supported transversely inhomogeneous functionally graded nanoplate in thermal environment using Rayleigh–Ritz method. *J. Vib. Control* **2021**, *27*, 2835–2847. [CrossRef]
16. Kaur, N.; Khanna, A.; Ozer, O. Thermoelastic Vibrational Analysis of Tapered Triangular Plates with Different Boundary Conditions. *Mech. Solids* **2023**, *58*, 1370–1377. [CrossRef]
17. Khanna, A.; Kaur, N. Theoretical Study on Vibration of Non-homogeneous Tapered Visco-Elastic Rectangular Plate. *Proc. Natl. Acad. Sci. USA* **2016**, *86*, 259–266. [CrossRef]
18. Sharma, A.K.; Bensal, S. Free vibration analysis of square structure plate with different boundary conditions. *Rom. J. Acoust. Vib.* **2023**, *20*, 13–26.
19. Khanna, A.; Kaur, N. Vibration of Non-Homogeneous Plate Subject to Thermal Gradient. *J. Low Freq. Noise, Vib. Act. Control* **2014**, *33*, 13–26. [CrossRef]
20. Bhardwaj, R.; Mani, N.; Sharma, A. Natural vibration of tapered rectangular plate with exponential variation in non-homogeneity. *J. Vibroeng.* **2019**, *21*, 187–197.
21. Sharma, A. Vibration Frequencies Of A Rectangular Plate With Linear Variation In Thickness And Circular Variation In Poisson's Ratio. *J. Theor. Appl. Mech.* **2019**, *57*, 605–615. [CrossRef] [PubMed]
22. Khanna, A.; Kaur, N. Effect of non-homogeneity on free vibration of visco-elastic rectangular plate with varying structural parameters. *J. Vibroeng.* **2013**, *15*, 2146–2155.
23. Khanna, A.; Kaur, N. Effect of structural parameters on the vibrational response of a visco-elastic rectangular plate with clamped ends. *Proc. Est. Acad. Sci. USA* **2015**, *64*, 127–138. [CrossRef]

Disclaimer/Publisher's Note: The statements, opinions and data contained in all publications are solely those of the individual author(s) and contributor(s) and not of MDPI and/or the editor(s). MDPI and/or the editor(s) disclaim responsibility for any injury to people or property resulting from any ideas, methods, instructions or products referred to in the content.